

## ARTICLE TYPE

## Simultaneous Vortex and Non-vortex based Transmission

Man Hee Lee | Hye Yeong Lee | Soo Young Shin

<sup>1</sup>Department of IT Convergence Engineering,  
Kumoh National Institute of Technology,  
Gyeongbuk, South Korea

## Correspondence

Corresponding author Soo Young Shin,  
Email: wdragon@kumoh.ac.kr

## Present address

M.H. Lee, H.Y. Lee and S.Y. Shin are with WENS  
Laboratory, Department of IT Convergence  
Engineering, Kumoh National Institute of  
Technology (e-mail: fordmore@kumoh.ac.kr;  
lhy413@kumoh.ac.kr; wdragon@kumoh.ac.kr).

## Abstract

In this paper, simultaneous vortex and non-vortex based transmission is proposed to enhance capacity by covering multiple users. The system model proposes a cell scenario including new and legacy user equipments (UEs) for backward compatibility and a geometrical transceiver for uniform circular array (UCA) and uniform rectangular array (URA). The proposed scenarios are divided into two different types of transmissions; vortex based, non-vortex based and a simultaneous vortex and non-vortex based. The channel model is approximated by dominant transmission distance. Moreover, modified Bessel function is proposed to derive channel model giving fair divergence effect with elevation angle. The performance of simultaneous vortex and non-vortex based transmissions is derived and simulated in terms of the average capacity (AC), outage probability (OP), and throughput.

## KEYWORDS

average capacity (AC), B5G, backward compatibility, outage probability (OP), throughput

## 1 | INTRODUCTION

Wireless communication systems have changed through a revolutionary paradigm from 3G to 5G, approximately every 10 years. Beyond 5G (B5G) and 6G represent the next generation of wireless communication technologies that focus on meeting the demand for high data rate, massive connectivity, and high reliability<sup>1,2,3</sup>. To achieve these demands, B5G/6G is expected to use interactive technologies such as massive multiple-input multiple-output (MIMO), beamforming, millimeter-wave (mmWave), and, orbital angular momentum (OAM)<sup>4,5</sup>.

OAM is a new wireless technology that has a high degree of freedom to increase the capacity significantly without requiring an additional spectrum or resources known as time, frequency and power<sup>6,7</sup>. OAM allows to use the vortex properties of electromagnetic waves. Hence, it is possible to transmit multiple independent data using its helical structure<sup>8</sup>. However, there are also several challenges such as misalignment and divergence. Despite of these challenges, OAM is an active research and development area because it is enable to evolve the speed and capacity of wireless communications.

MIMO is another technique in wireless communication because it increases data rate and improves link reliability and spectral efficiency (SE)<sup>9,10</sup>. However, there are also several challenges such as synchronization and interference between transmitter and receiver. Despite of these challenges, MIMO has achieved a high SE through the use of spatial diversity and spatial multiplexing to collect channel state information. Overall, the interaction between MIMO (i.e. non-vortex based transmission) and OAM (i.e. vortex based transmission) is expected to improve the SE in the sense of using multiple antenna elements.

Generally, antenna types are divided into uniform linear array (ULA), uniform circular array (UCA) and uniform rectangular array (URA)<sup>11,12</sup>. The UCA has been recommended as a promising antenna type for vortex based transmission because of its advantages in terms of cost, size, and flexibility. In addition, UCA is an important antenna type in vortex based transmission to generate multiple helical phases<sup>13,14</sup>. In contrast, a URA and a ULA have commonly used as antenna types for non-vortex based transmission<sup>15</sup>. A URA is equipped in base station (BS) for cellular communication because it can provide high gain and large coverage. Otherwise, a ULA is used in satellite and aircraft because it has benefit in size and complexity<sup>16</sup>.

There are many researches on the non-vortex based transmission by configuring different antenna types. In<sup>17</sup>, many different configurations and deployment scenarios have shown for a massive MIMO. A URA served a single terminal, a cylindrical antenna using maximum ratio combining served multiple terminals, and a ULA using zero-forcing served also multiple terminals. The relationship between energy efficiency and SE was derived to compare different antenna types. In<sup>18</sup>, the guidelines were presented for choosing the appropriate antenna types such as UCA, URA, and ULA according to communication scenarios and requirements. Channel models were derived with azimuth and elevation angles of arrival at the same path point. However, the research on the vortex based transmission is limited in<sup>19</sup>, both UCA-OAM and UCA-MIMO are compared in terms of SE and feedback overhead. The results included the relationship between the eigenmodes of UCA-MIMO and the modes of UCA-OAM as well as the capacity formula. However, the system models were separated using OAM and MIMO.

while efforts are being worked on the vortex-based transmission, it is necessary to take care of the backward compatibility in scenarios where new and legacy devices coexist. For example, the existing wireless access standards including IEEE 802.11a, 802.11n, and 802.11ac shares technical characteristics<sup>20</sup>. In addition, the possibility generating vortex beams from URA has revealed by decomposing UPA into a superposition of UCA<sup>21</sup>. This paper will highlight the potential benefits with simultaneous vortex and non-vortex based transmission with feasibility decomposing URA into UCA. To achieve enhance the capacity and backward compatibility by supporting multiple types of antennas, a BS is required to compose a mixture of antennas, such as a combination of UCAs and URAs.

The summary contributions of this paper are as follows

- Simultaneous vortex and non-vortex based transmission is proposed to cover multiple UEs (new and legacy)
- The element distance is derived based on the coordinates between transmitter and receiver
- Line-of-sight (LoS) channel models are approximated and derived with modified Bessel function for legacy and new UEs
- Three scenarios (S1,S2,S3) are considered to compare the vortex and non-vortex based transmission according to different types of antennas and a mixture of antennas (S1: only vortex based, S2: only non-vortex based, S3: simultaneous vortex and non-vortex based)
- The performance is derived and validated with regard to the average capacity (AC), outage probability (OP), and throughput

The remainder of this paper is organized as follows. Section 2 discusses the vortex and non-vortex based transmission model with a geometrical transceiver and a channel model. In Section 3, three scenarios are presented considering new user equipment (NUE) and legacy user equipment (LUE). The performance metrics are introduced in Section 4 including the average capacity (AC), outage probability (OP) and throughput. In Section 5, numerical results are compared under the given conditions and parameters. The conclusion drawn from this paper is presented in Section 6.

## 2 | VORTEX AND NON-VORTEX BASED TRANSMISSION MODEL

In this section, the vortex and non-vortex based transmission model is described in detail. The geometrical transceivers for UCA and URA are shown in the Figure. 1. The components of UCA include the transmit UCA (TUCA) element, receive UCA (RUCA) element, radius of TUCA or RUCA, azimuthal angle of TUCA/RUCA and center distance between TUCA and RUCA. Thus, the components of URA represent the transmit URA (TURA) element, receive URA (RURA) element, element interval of TURA or RURA and center distance between TURA and RURA. The notations of these components are summarized in the Table 1.

Let us indicate the center of TUCA with the coordinates (0,0,0) on the xyz plane. The coordinates of the  $n$ -th element on the TUCA ( $A$ )<sub>v</sub>, the center of the RUCA ( $B$ )<sub>v</sub>, and the  $m$ -th element on the RUCA ( $C$ )<sub>v</sub> are represented as follows

$$\begin{aligned} (A_x, A_y, A_z)_v &= (r \sin \varphi_n, r \cos \varphi_n, 0) \\ (B_x, B_y, B_z)_v &= (0, d_v \sin \phi_v, d_v \cos \phi_v) \\ (C_x, C_y, C_z)_v &= (R \sin \varphi_m, R \cos \varphi_m + d_v \sin \phi_v, d_v \cos \phi_v) \end{aligned} \quad (1)$$

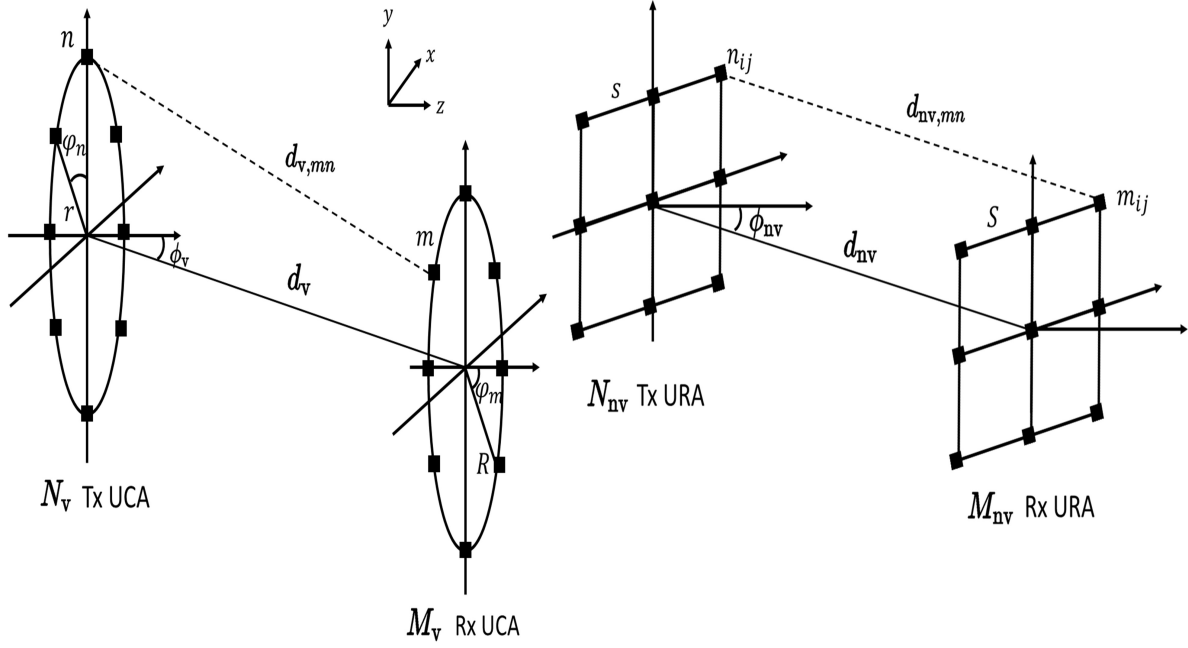


**FIGURE 1** Geometrical transceivers for UCA and URA.

**TABLE 1** List of Symbols used in this paper

Symbol	Definition
$N_v$	Number of TUCA elements
$M_v$	Number of RUCA elements
$r$	Radius of TUCA
$R$	Radius of RUCA
$\varphi_n = 2\pi(n-1)/N_v$	Azimuthal angle of TUCA
$\varphi_m = 2\pi(m-1)/M_v$	Azimuthal angle of RUCA
$\phi_v$	Elevation angle of UCA
$d_v$	Center distance between UCAs
$d_{v,mn}$	Element distance between UCAs
$N_{nv}$	Number of TURA elements
$M_{nv}$	Number of RURA elements
$s$	Element spacing of TURA
$S$	Element spacing of RURA
$n_i$	Number of rows on TURA element (x plane)
$n_j$	Number of columns on TURA element (y plane)
$m_i$	Number of rows on RURA element (x plane)
$m_j$	Number of columns on RURA element (y plane)
$\phi_{nv}$	Elevation angle of URA
$d_{nv}$	Center distance between URAs
$d_{nv,mn}$	Element distance between URAs

Let us indicate the center of TURA with the coordinate  $(0,0,0)$  on the  $xyz$  plane. The coordinates of the  $n$ -th element on the TURA  $(A)_{nv}$ , the center of RURA  $(B)_{nv}$ , and the  $m$ -th element on the RURA  $(C)_{nv}$  are represented as follows

$$\begin{aligned}
 (A_x, A_y, A_z)_{nv} &= (s(n_i - 1), s(n_j - 1), 0) \\
 (B_x, B_y, B_z)_{nv} &= (0, d_{nv} \sin \phi_{nv}, d_{nv} \cos \phi_{nv}) \\
 (C_x, C_y, C_z)_{nv} &= (S(m_i - 1), d_{nv} \sin \phi_{nv} + S(m_j - 1), d_{nv} \cos \phi_{nv})
 \end{aligned} \tag{2}$$

For the vortex based channel model, these coordinates are used to calculate the element distance between the TUCA and RUCA<sup>22</sup>. This can be written as follows

$$\begin{aligned}
 d_{v,mn} &= \sqrt{(C_x - A_x)_v^2 + (C_y - A_y)_v^2 + (C_z - A_z)_v^2} \\
 &= \sqrt{r^2 + R^2 + d_v^2 + 2(\mathcal{P}_{v,m} + \mathcal{F}_{v,mn} + \mathcal{W}_{v,n})} \\
 &\begin{cases} \mathcal{P}_{v,m} = d_v R \sin \phi_v \cos \varphi_m \\ \mathcal{F}_{v,mn} = -r R \cos(\varphi_m - \varphi_n) \\ \mathcal{W}_{v,n} = -d_v r \sin \phi_v \cos \varphi_n \end{cases}
 \end{aligned} \tag{3}$$

For the non-vortex based channel model, the above coordinates are used to calculate the element distance between TURA and RURA and can be written as follows

$$\begin{aligned}
 d_{nv,mn} &= \sqrt{(C_x - A_x)_{nv}^2 + (C_y - A_y)_{nv}^2 + (C_z - A_z)_{nv}^2} \\
 &= \sqrt{d_{nv}^2 + d_{nv,i}^2 + d_{nv,j}^2 + 2d_{nv}d_{nv,j} \sin \phi_m} \\
 &\begin{cases} d_{nv,i} = S(m_i - 1) - s(n_i - 1) \\ d_{nv,j} = S(m_j - 1) - s(n_j - 1) \end{cases}
 \end{aligned} \tag{4}$$

The element distance for UCAs and URAs must change their form to derive the dominant parameters. Hence, the element distances ( $d_{v,mn}, d_{nv,mn}$ ) for the vortex based and non-vortex based transmissions can be rewritten and approximated as follows

$$\begin{aligned}
 d_{v,mn} &= \sqrt{r^2 + R^2 + d_v^2} \sqrt{1 + \frac{2(\mathcal{P}_{v,m} + \mathcal{F}_{v,mn} + \mathcal{W}_{v,n})}{r^2 + R^2 + d_v^2}} \\
 &\stackrel{(a)}{\approx} \sqrt{r^2 + R^2 + d_v^2} \left( 1 + \frac{\mathcal{P}_{v,m} + \mathcal{F}_{v,mn} + \mathcal{W}_{v,n}}{r^2 + R^2 + d_v^2} \right) \\
 &\stackrel{(b)}{\approx} d_v \left( 1 + \frac{\mathcal{P}_{v,m} + \mathcal{F}_{v,mn} + \mathcal{W}_{v,n}}{d_v^2} \right) \\
 \hat{d}_{v,mn} &\stackrel{(b)}{\approx} d_v + \frac{\{R \sin \phi_v \cos \varphi_m - r \sin \phi_v \cos \varphi_n\}}{d_v} \\
 d_{nv,mn} &= \sqrt{d_{nv}^2 + d_{nv,i}^2 + d_{nv,j}^2} \sqrt{1 + \frac{2d_{nv}d_{nv,j} \sin \phi_{nv}}{d_{nv}^2 + d_{nv,i}^2 + d_{nv,j}^2}} \\
 \hat{d}_{nv,mn} &\stackrel{(a),(b)}{\approx} d_{nv} + \frac{d_{nv,j} \sin \phi_{nv}}{d_{nv}},
 \end{aligned} \tag{5}$$

where (a) follows the binomial approximation  $\sqrt{1+x} \approx 1+x/2$  from<sup>23</sup> and (b) follows the condition  $d_v \gg r, R$  and  $d_{nv} \gg d_{nv,i}, d_{nv,j}$ . Furthermore, the channel model for vortex and non-vortex based transmissions considers the LoS channel that can be derived<sup>24</sup>.

The LoS channel model for vortex and non-vortex based transmissions can be obtained using (5) as follows

$$\begin{aligned}
 h(\hat{d}_{v,mn}) &= \beta \frac{\lambda_v}{4\pi \hat{d}_{v,mn}} e^{-j \frac{2\pi}{\lambda_v} \hat{d}_{v,mn}} \\
 &= \beta \frac{\lambda_v}{4\pi \hat{d}_{v,mn}} e^{-j \frac{2\pi}{\lambda_v} d_v} e^{-j \frac{2\pi}{\lambda_v} \frac{R \sin \phi_v \cos \varphi_m - r \sin \phi_v \cos \varphi_n}{d_v}} \\
 &\approx \beta \frac{\lambda_v}{4\pi d_v} e^{-j \frac{2\pi}{\lambda_v} d_v} e^{-j \frac{2\pi}{\lambda_v} \frac{R \sin \phi_v \cos \varphi_m - r \sin \phi_v \cos \varphi_n}{d_v}} \\
 h(\hat{d}_{nv,mn}) &\approx \beta \frac{\lambda_{nv}}{4\pi d_{nv}} e^{-j \frac{2\pi}{\lambda_{nv}} d_{nv}} e^{-j \frac{2\pi}{\lambda_{nv}} \frac{d_{nv,j} \sin \phi_{nv}}{d_{nv}}}
 \end{aligned} \tag{6}$$

where  $\lambda_v, \lambda_{nv}$  are the wavelengths of the carrier frequency for vortex and non-vortex based transmissions.  $\beta$  denotes the small-scale fading factor, which is related to antenna elements and patterns. The approximation of the element distance can be converted into the center distance because of its overwhelming out of the exponential function. Furthermore, element distance can be estimated from transmission distance with azimuthal angle and radius of antenna. Hence, the free space loss  $\lambda_v/4\pi d_v$  or  $\lambda_{nv}/4\pi d_{nv}$  can be represented as a large-scale fading factor. Note that NLoS channel can be considered and derived from LoS channel model by adding multi-path component<sup>25</sup>.

In<sup>26</sup>, it is known that the multiplication of discrete Fourier transform (DFT) and inverse DFT (IDFT) with the vortex based channel matrix yields a diagonal matrix because DFT and IDFT matrices are unitary. The DFT is a part of the receive matrix and the IDFT is a part of the transmit matrix to detect OAM mode information. Therefore, the entire channel matrix for the vortex based transmission can be expressed as follows

$$\begin{aligned} \mathbf{h}_v &= \sum_{n=1}^{N_v} \frac{1}{\sqrt{N_v}} e^{-jl\varphi_n} h(\hat{d}_{v,mn}) \sum_{m=1}^{M_v} \frac{1}{\sqrt{M_v}} e^{jl\varphi_m} \\ &= \beta \frac{\lambda_v}{4\pi d_v \sqrt{N_v} \sqrt{M_v}} e^{-j\frac{2\pi}{\lambda_v} d_v} \mathcal{B}_t \mathcal{B}_r (2\pi)^2 \\ &\stackrel{(c)}{\approx} \beta \frac{\lambda_v \pi N_v M_v}{d_v \sqrt{N_v} \sqrt{M_v}} e^{-j\frac{2\pi}{\lambda_v} d_v} \mathcal{I}_l \left( \frac{2\pi r \sin \phi_v}{d_v \lambda_v} \right) \mathcal{I}_l \left( \frac{2\pi R \sin \phi_v}{d_v \lambda_v} \right), \end{aligned} \quad (7)$$

where  $\mathcal{B}_t$  and  $\mathcal{B}_r$  can be represented as

$$\begin{aligned} \mathcal{B}_t &= \frac{1}{2\pi} \sum_{n=1}^{N_v} e^{jl(-\varphi_n)} e^{j\frac{2\pi r \sin \phi_v}{d_v \lambda_v} \cos(-\varphi_n)} \\ \mathcal{B}_r &= \frac{1}{2\pi} \sum_{m=1}^{M_v} e^{jl\varphi_m} e^{j\frac{2\pi R \sin \phi_v}{d_v \lambda_v} \cos \varphi_m} \end{aligned} \quad (8)$$

where Eq. (7), (c) follows the transformation from an infinite series to a definite integral<sup>27</sup> using the modified Bessel function  $\mathcal{I}_l(x) \equiv (2\pi)^{-1} \int_0^{2\pi} e^{jl\tau} e^{jx \cos \tau} d\tau$ . Note that the modified Bessel function is used to give fair divergence effect on channel model according to<sup>28</sup>. Based on the approximations, the channel model is represented with transmission distance which is dominant parameter i.e. center distance.

For the non-vortex based channel model, the DFT and IDFT can be applied where the mode number for vortex based ( $l = 0$ ) is assigned as a precoding purpose<sup>19</sup>. This multiplication also yields the transformation from a channel matrix to a diagonal matrix by removing the determinant parameters from other elements as similar to the vortex based channel model. Therefore, the entire channel matrix for the non-vortex based transmission can be expressed as follows

$$\begin{aligned} \mathbf{h}_{nv} &= \sum_{n=1}^{N_{nv}} \frac{1}{\sqrt{N_{nv}}} e^{-j0\varphi_n} h(\hat{d}_{nv,mn}) \sum_{m=1}^{M_{nv}} \frac{1}{\sqrt{M_{nv}}} e^{j0\varphi_m} \\ &= \sqrt{N_{nv} M_{nv}} h(\hat{d}_{nv,mn}) \\ &= \beta \frac{\lambda_{nv} \sqrt{N_{nv} M_{nv}}}{4\pi d_{nv}} e^{-j\frac{2\pi}{\lambda_{nv}} d_{nv}} e^{-j\frac{2\pi}{\lambda_{nv}} \frac{\{S(m_j-1)-s(n_j-1)\} \sin \phi_{nv}}{d_{nv}}}, \end{aligned} \quad (9)$$

This is an effective approach to analyze multiple NUES and LUES in the same manner. The details of NUES and LUES are described in Section 3.

### 3 | PROPOSED SCENARIOS: COEXISTENCE OF NUES AND LUES

In this section, three scenarios are initially presented and described to analyze the simultaneous vortex and non-vortex based transmissions. A mixture of antenna types for BS supports NUES and LUES and the effect of the given scenarios shows how to determine the optimal solution. In Figure. 2, we propose a cell scenario comprising a single base station (BS), multiple NUES, and LUES. The BS is equipped with compatible antennas that can simultaneously communicate with  $K_o$  number of NUES and  $K_m$  number of LUES. Note that NUES and LUES are divided by the use of frequency bands such as above-6GHz and sub-6GHz. According to the cell scenario, the BS compromises vortex and non-vortex based transmissions by assigning two types of antennas such as UCA and ULA.

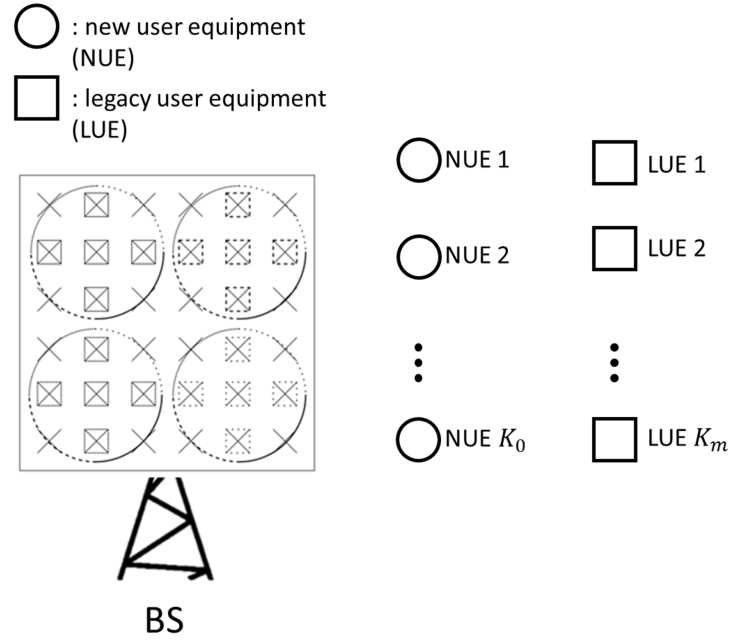


**FIGURE 2** A cell scenario.

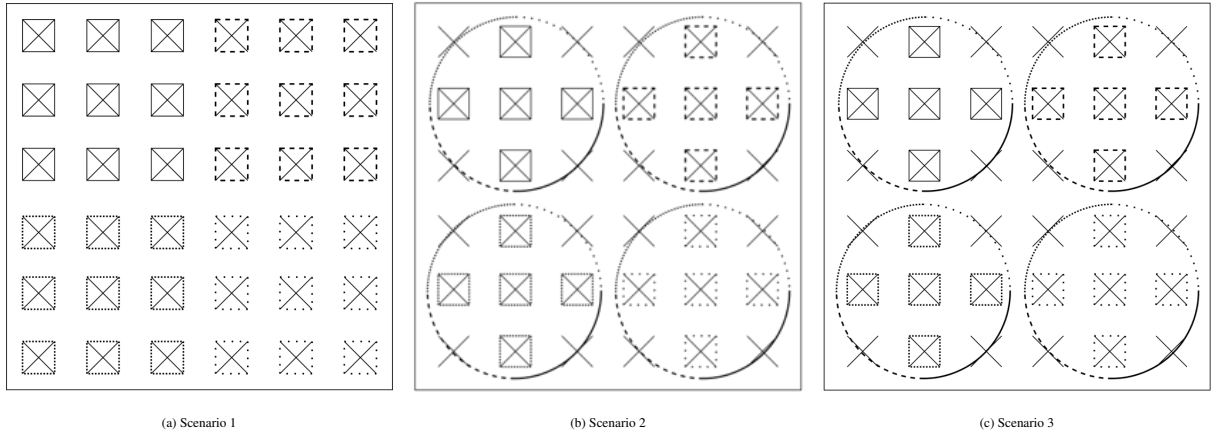


**FIGURE 3** Proposed scenarios

The same conditions such antenna element spacing and the total number of antenna element are given for  $K_o$  number of NUEs and  $K_m$  number of LUEs. The URA elements are divided into  $K_m$  number of LUEs for the non-vortex based transmission, whereas the UCA elements are divided into  $K_o$  number of NUEs with  $L$  OAM modes. Finally, three scenarios are divided and designed as shown in Figure. 3. The total number of antenna elements from BS are based on the number of TURA elements,  $N_{nv}$ . In Scenario 1 (S1) and Scenario 2 (S2),  $K_m$  LUEs and  $K_o$  NUEs are supported separately, while both LUEs and NUEs are supported in Scenario 3 (S3). Hence, S3 can support a higher number of users than that of S2 and S3. Additionally, it covers backward compatibility, which is maintained by different types of antennas and communication schemes.

### 3.1 | Scenario 1: LUEs only

In the first scenario of Fig. 3a,  $N_{nv}$  number of TURA elements on the BS are configured to communicate with  $K_m$  LUEs. Each LUE has  $M_{nv}$  number of RURA elements. The transmission distance is represented as  $d_{nv}$  between the BS and LUE  $k_m (m = 1, \dots, 4)$ . The channel model for the non-vortex based transmission follows  $\mathbf{h}_{nv,k}$  for each LUE.

### 3.2 | Scenario 2: NUEs only

In the second scenario of Fig. 3b,  $N_v$  number of TURA elements on the BS are configured to communicate with  $K_o$  NUEs. Each NUE has  $M_v$  number of RUCA elements. To be specific, it is considered that every antenna element has phase shifter to generate vortex based communication. The transmission distance is represented as  $d_v$  between the BS and NUE  $k_o (o = 1, \dots, 4)$ . The channel model for the vortex based follows  $\mathbf{h}_{v,k}$  with  $L$  number of OAM modes for each NUE.

### 3.3 | Scenario 3: both LUEs and NUEs

In the third scenario of Fig. 3c,  $(N_{nv} - N_v)$  number of TURA elements and  $N_v$  number of TUCA elements on the BS are configured to communicate with  $K_m$  LUEs and  $K_o$  NUEs. LUE and NUE have  $M_{nv}$  number of RURA elements and  $M_v$  number of RUCA elements, respectively. The distance condition for  $k_m$  and  $k_o$  are the same as those for S1 and S2. However, the radii of TUCAs are increased and the number of TURA elements is reduced compared to that of S1 and S2. The mixture of UCAs and URAs provides flexible radius of UCAs and number of URA elements.

From the above scenarios, the scenario condition is considered that every NUE is closer than every LUE because different carrier frequency bands of NUEs and LUEs are assigned to the above-6GHz (30GHz) and sub-6GHz (5GHz), respectively. The characteristic of electromagnetic waves is considered because of entire antenna size is fixed. In this paper, the utilization of different hardware or software allows backward compatibility to support different carrier frequency bands.

## 4 | PERFORMANCE ANALYSIS

In this section, the proposed simultaneous vortex and non-vortex based transmission is analyzed and discussed in terms of the average capacity (AC), outage probability (OP) and throughput. The AC, OP and throughput of simultaneous vortex and non-vortex based transmissions are analyzed and compared with those of non-vortex based transmission and vortex based transmission.

### 4.1 | Average capacity analysis

Let us consider S1 and S2 for the two cases that non-vortex and vortex based transmission supports LUEs and NUEs, separately. Otherwise, simultaneous non-vortex and vortex based transmission supports the coexistence of LUEs and NUEs as shown in S3. The AC for each scenario is calculated as follows

$$\begin{aligned} C_1 &= \sum_{k=1}^{K_m} \mathbb{E} \left\{ \log_2 \left( 1 + \frac{\rho \sum_{\mathcal{L}} |\mathbf{h}_{nv,k}|^2}{N_m \sigma^2} \right) \right\} \\ C_2 &= \sum_{k=1}^{L_2} \sum_{k=1}^{K_o} \mathbb{E} \left\{ \log_2 \left( 1 + \frac{\rho |\mathbf{h}_{v,k}|^2}{N_o \sigma^2} \right) \right\} \\ C_3 &= C_1 + \sum_{k=1}^{L_3} \sum_{k=1}^{K_o} \mathbb{E} \left\{ \log_2 \left( 1 + \frac{\rho |\mathbf{h}_{v,k}|^2}{N_o \sigma^2} \right) \right\}, \end{aligned} \quad (10)$$

where  $\mathbb{E}\{\cdot\}$  is the expectation operation and  $\rho$  is the transmit signal-to-noise ratio (SNR).  $\mathcal{L}$  is the number of multi-path and  $\sigma$  denotes the additive Gaussian noise variance.  $N_v$  and  $N_{nv}$  are the numbers of TUCA and TURA elements for LUEs and NUEs, respectively.  $L_2 \in \{-l, \dots, 0, \dots, l\}$  and  $L_3 \in \{-l, \dots, l\}, l \neq 0$  represents the combination of OAM modes for S2 and S3. Note

that vortex and non-vortex based transmission has no inter-beam interference theoretically where vortex based transmission do not use mode zero. The AC for S3 does not include the interference term because there is no inter-beam interference.

## 4.2 | Outage probability analysis

The OP is derived in closed form for S1, S2 and S3. The cumulative distribution function (CDF) of the transmit SNR is evaluated using the rate threshold,  $\Gamma_{th}$ . Additionally, the OP includes connectivity errors between the BS and UEs under varying channel conditions. The power of exponential satisfies the conversion from CDF to probability density function (PDF)<sup>29</sup>. The asymptotic approach can be used for SNR approximation where  $\exp(x) \approx 1 + x$  for  $x \rightarrow 0$ . The exact and asymptotic OP for S1, S2, and S3 including connectivity error can be derived as follows

$$\begin{aligned} F_{\alpha}^{\text{ext}} &= \epsilon_{\alpha} [\mathbf{P}_r \{(2^{C_{\alpha}} - 1) \leq \Gamma_{th}\}] \\ &= \epsilon_{\alpha} [1 - \mathbf{P}_r \{(2^{C_{\alpha}} - 1) \geq \Gamma_{th}\}] \\ &= \epsilon_{\alpha} \left[ 1 - \exp \left( -\frac{\Gamma_{th}}{\rho \zeta_{\alpha}} \right) \right] \\ F_{\alpha}^{\text{asym}} &= \epsilon_{\alpha} \left( \frac{2^{C_{\alpha}} - 1}{\rho \zeta_{\alpha}} \right), \quad \forall \alpha = 1, 2 \\ F_3^{\text{ext}} &= \mathbb{E} \left[ (\epsilon_1 + \epsilon_2) \left\{ 1 - \exp \left( -\frac{\Gamma_{th}}{\rho \zeta_3} \right) \right\} \right], \end{aligned} \quad (11)$$

where  $\zeta_1$  and  $\zeta_2$  are the mean of the channels  $|\mathbf{h}_{nv}|^2$  and  $|\mathbf{h}_v|^2$ , respectively.  $C_1, C_2$ , and  $C_3$  are the ratio of AC to calculate outage.  $\epsilon_{\alpha}$  can be replaced into  $\epsilon_m$  or  $\epsilon_o$ , represent connectivity errors for non-vortex and vortex based transmission, respectively. This parameter can be named as a stability measurement because all of proposed antenna types can be switched at given conditions.

## 4.3 | Throughput analysis

The throughput refers to the delivery of a finite data rate over a communication channel. This is one of the basic measurements of the efficiency of the communication channels. The trade-off between AC and OP can be considered at the same time as the throughput<sup>30</sup>. Thus, the CDF based exact and asymptotic throughput for S1, S2, and S3 including connectivity error can be written as

$$\begin{aligned} \tau_{\alpha}^{\text{ext}} &= (1 - F_{\alpha}^{\text{ext}}) = (2^{C_{\alpha}} - 1) \exp \left( -\frac{(2^{C_{\alpha}} - 1)}{\rho \zeta_{\alpha}} \right) \\ \tau_{\alpha}^{\text{asym}} &= (1 - F_{\alpha}^{\text{asym}}) = (2^{C_{\alpha}} - 1) \left( 1 - \frac{2^{C_{\alpha}} - 1}{\rho \zeta_{\alpha}} \right), \quad \forall \alpha = 1, 2 \\ \tau_3^{\text{ext}} &= \mathbb{E} \left[ (\epsilon_1 + \epsilon_2) \left( 1 - \frac{2^{C_3} - 1}{\rho \zeta_3} \right) \right], \end{aligned} \quad (12)$$

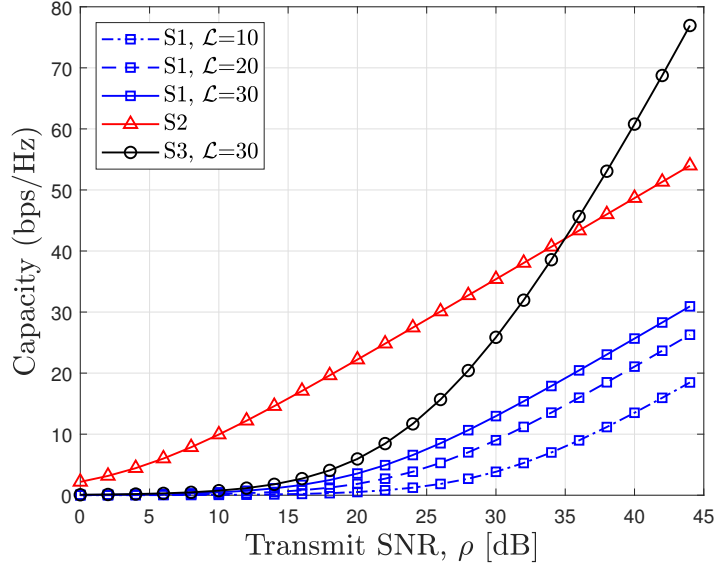
where the target capacity  $C_p$  is calculated from (10) varying with the transmit SNR.

## 5 | NUMERICAL RESULTS

In this section, we present simulated and analytical results to demonstrate the proposed scenarios. The performance metric deals with AC, OP and throughput. The simulation parameters are listed in the Table 2. The radii of UCAs and the element spacing of URAs can be varied according to the given scenarios. The number of NUEs and LUEs are fixed at four for fairness comparison between scenarios. In Figure. 4, the AC is shown with respect to the transmit SNR. As can be seen, the AC for S3 outperforms the other scenarios after 35 [dB] because the vortex based transmission has a non-linear slope, increasing the transmit SNR. The vortex based transmission has high benefit where transmit SNR is satisfied because vortex based transmissions has a divergence issue in low transmit SNR. In Figure. 5, the OP is shown with respect to the transmit SNR. The asymptotic and exact analysis for OP is shown for comparison with the given scenarios. Unlike AC, the OP for S2 shows better performance than the other scenarios (S1 and S3) because achievable outage ratio for S2 is higher than that for S1 and S3 compared with the mean of

**TABLE 2** Simulation parameters

Parameter	Value
Wavelength for vortex	$\lambda_v = 0.01$
Wavelength for non-vortex	$\lambda_{nv} = 0.1667$
Transmit SNR	$\rho = 40$ to $70$ dB
Transmission distances for NUEs	$d_{v,1} = 40, d_{v,2} = 45, d_{v,3} = 50, d_{v,4} = 60$
Transmission distances for LUEs	$d_{nv,1} = 70, d_{nv,2} = 75, d_{nv,3} = 80, d_{nv,4} = 90$
Elevation angles	$\phi_{nv} = \phi_v = 20^\circ, 10^\circ, -10^\circ, -30^\circ$
The number of multi-path	$\mathcal{L} = 10, 20, 30$
OAM modes	$-2, -1, 0, 1, 2$

**FIGURE 4** Average capacity comparison between scenarios.

channels. In addition, the OP gap between S2 and S3 is decreased after 40 [dB] because the OP is calculated by achievable outage ratio. In Figure. 6, the OP is shown with respect to transmit SNR with assigning different connectivity errors between vortex and non-vortex based transmissions. The connectivity parameters such as  $\epsilon_m$  and  $\epsilon_o$  is given from 1 (stable) to 2 (unstable). The connectivity errors occurs higher errors compared with Figure. 5. To analysis the numerical results of S3, magnified figure is shown that the effect of connectivity parameters are equal on the OP of S3 (circle and plus sign markers, right triangle and diamond markers).

In Figure. 7, the throughput is shown with respect to transmit SNR for the given scenarios. The maximum workload for the throughput is fixed as 1 where the given SNR is 45 [dB] because we assume that the AC is normalized at that SNR. The throughput for S2 shows better performance than the other scenarios (S1 and S3) because the AC for S2 is higher than that for S1 and S3.

In Figure 8, the throughput is shown with respect to transmit SNR with assigning different connectivity errors between vortex and non-vortex based transmissions. To analysis the numerical results of S3, magnified figure is shown that the effect of connectivity errors is same with the OP according to given parameters. However, the achievable outage ratio has higher effect on throughput than OP.

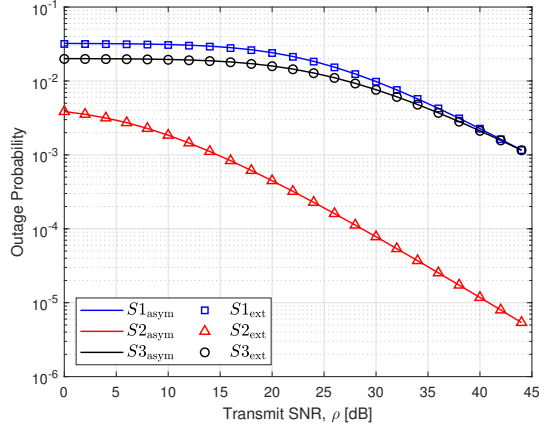


FIGURE 5 Outage probability comparison between scenarios.

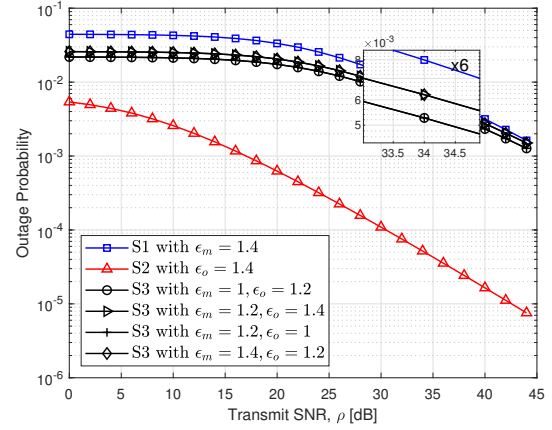


FIGURE 6 Outage probability comparison with connectivity error.

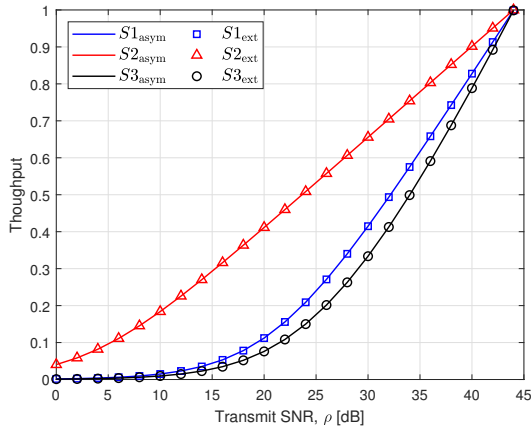


FIGURE 7 Throughput comparison between scenarios.

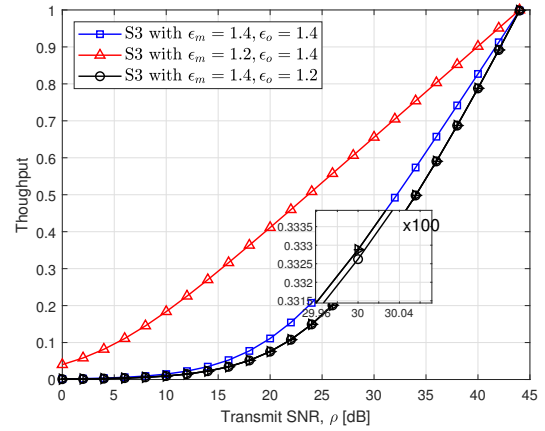


FIGURE 8 Throughput comparison with connectivity error.

## 6 | CONCLUSION

In this paper, simultaneous vortex and non-vortex based transmission is proposed to enhance the AC for future wireless network. Different scenarios are considered where both LUEs (non-vortex) and NUEs (vortex) are coexisted for backward compatibility. The channel models for vortex and non-vortex based transmissions are derived in mathematical approach with modified Bessel function. Both analytic and simulation results shows the effectiveness of the proposed simultaneous vortex and non-vortex based transmission. Finding the optimal user grouping and applying optimization algorithm for enhancing capacity could be future works.

## CONFLICT OF INTEREST

The authors declare no potential conflict of interests.

## REFERENCES

1. Saad W, Bennis M, Chen M. A vision of 6G wireless systems: Applications, trends, technologies, and open research problems. *IEEE network*. 2019;34(3):134–142.
2. Hakeem SAA, Hussein HH, Kim H. Vision and research directions of 6G technologies and applications. *Journal of King Saud University-Computer and Information Sciences*. 2022.
3. Dwivedi B, Sen D, Chakraborty S. A survey of longitudinal changes in cellular network architecture: The good, the bad, and the ugly. *Journal of Network and Computer Applications*. 2022:103496.

4. Mohammadi SM, Daldorff LK, Bergman JE, et al. Orbital angular momentum in radio—A system study. *IEEE transactions on Antennas and Propagation*. 2009;58(2):565–572.
5. Trichili A, Park KH, Zghal M, Ooi BS, Alouini MS. Communicating using spatial mode multiplexing: Potentials, challenges, and perspectives. *IEEE Communications Surveys & Tutorials*. 2019;21(4):3175–3203.
6. Edfors O, Johansson AJ. Is orbital angular momentum (OAM) based radio communication an unexploited area?. *IEEE Transactions on Antennas and Propagation*. 2011;60(2):1126–1131.
7. Sawant A, Lee I, Jung BC, Choi E. Ultimate capacity analysis of orbital angular momentum channels. *IEEE Wireless Communications*. 2020;28(1):90–96.
8. Chen R, Zhou H, Moretti M, Wang X, Li J. Orbital angular momentum waves: generation, detection, and emerging applications. *IEEE Communications Surveys & Tutorials*. 2019;22(2):840–868.
9. Xiao Z, Han Z, Nallanathan A, et al. Antenna array enabled space/air/ground communications and networking for 6g. *IEEE Journal on Selected Areas in Communications*. 2022;40(10):2773–2804.
10. Zhang H, Shlezinger N, Guidi F, Dardari D, Imani MF, Eldar YC. Beam focusing for near-field multiuser MIMO communications. *IEEE Transactions on Wireless Communications*. 2022;21(9):7476–7490.
11. Chang DC, Hu CN. Smart antennas for advanced communication systems. *Proceedings of the IEEE*. 2012;100(7):2233–2249.
12. Ai B, Cheng X, Kürner T, et al. Challenges toward wireless communications for high-speed railway. *IEEE transactions on intelligent transportation systems*. 2014;15(5):2143–2158.
13. Gong Y, Wang R, Deng Y, et al. Generation and transmission of OAM-carrying vortex beams using circular antenna array. *IEEE Transactions on antennas and propagation*. 2017;65(6):2940–2949.
14. Feng PY, Qu SW, Yang S. OAM-generating transmitarray antenna with circular phased array antenna feed. *IEEE Transactions on Antennas and Propagation*. 2020;68(6):4540–4548.
15. Mahmood M, Koc A, Le-Ngoc T. Energy-efficient MU-massive-MIMO hybrid precoder design: Low-resolution phase shifters and digital-to-analog converters for 2D antenna array structures. *IEEE Open Journal of the Communications Society*. 2021;2:1842–1861.
16. Johnson DH, Dudgeon DE. *Array signal processing: concepts and techniques*. Prentice Hall., 1993.
17. Larsson EG, Edfors O, Tufvesson F, Marzetta TL. Massive MIMO for next generation wireless systems. *IEEE communications magazine*. 2014;52(2):186–195.
18. Cheng X, He Y, Qiao J. Channel modeling for UCA and URA massive MIMO systems. In: IEEE. 2020:963–968.
19. Gil GT, Lee JY, Kim H, Cho DH. Comparison of UCA-OAM and UCA-MIMO systems for sub-THz band line-of-sight spatial multiplexing transmission. *Journal of Communications and Networks*. 2021;23(2):83–90.
20. Dhawankar P, Kumar A, Crespi N, et al. Next-Generation Indoor Wireless Systems: Compatibility and Migration Case Study. *IEEE Access*. 2021;9:156915–156929.
21. Cho H, Park C, Lee N. Capacity-achieving precoding with low-complexity for terahertz LOS massive MIMO using uniform planar arrays. In: IEEE. 2020:535–539.
22. Jing H, Cheng W, Xia XG. A simple channel independent beamforming scheme with parallel uniform circular array. *IEEE Communications Letters*. 2019;23(3):414–417.
23. Griffiths DJ. *Introduction to electrodynamics*. 2005.
24. Zhou J, Cheng W, Liang L. OAM transmission in sparse multipath environments with fading. In: IEEE. 2020:1–6.
25. Raghavan V, Sayeed AM. Sublinear capacity scaling laws for sparse MIMO channels. *IEEE Transactions on Information Theory*. 2010;57(1):345–364.
26. Kushel O, Tyaglov M. Circulants and critical points of polynomials. *Journal of Mathematical Analysis and Applications*. 2016;439(2):634–650.
27. Abramowitz M, Stegun IA. *Handbook of mathematical functions with formulas, graphs, and mathematical tables*. 55. US Government printing office, 1948.
28. Lee MH, Lee HY, Shin SY. Divergence Intensity and Mode Combinations for Multiple OAM users. 2022.
29. Ozduran V. Inverse successive interference cancellation for non-orthogonal multiple access. In: IEEE. 2019:1–4.
30. LEE MH, SHIN SY. On the performance analysis of flexible pairing between UAV and GU in NOMA. *Turkish Journal of Electrical Engineering and Computer Sciences*. 2022;30(5):1715–1725.